Journal of
Applied Remote Sensing

RemoteSensing.SPIEDigitalLibrary.org

Demonstration of 25-Hz-inspection-speed laser remote sensing for internal concrete defects

Shinri Kurahashi
Katsuhiro Mikami
Toshiyuki Kitamura
Noboru Hasegawa
Hajime Okada
Shuji Kondo
Masaharu Nishikino
Tetsuya Kawachi
Yoshinori Shimada

SPIE.

Shinri Kurahashi, Katsuhiro Mikami, Toshiyuki Kitamura, Noboru Hasegawa, Hajime Okada, Shuji Kondo, Masaharu Nishikino, Tetsuya Kawachi, Yoshinori Shimada, "Demonstration of 25-Hz-inspection-speed laser remote sensing for internal concrete defects," *J. Appl. Remote Sens.* **12**(1), 015009 (2018), doi: 10.1117/1.JRS.12.015009.

Demonstration of 25-Hz-inspection-speed laser remote sensing for internal concrete defects

Shinri Kurahashi,[a,*] Katsuhiro Mikami,[b] Toshiyuki Kitamura,[a,b] Noboru Hasegawa,[b] Hajime Okada,[b] Shuji Kondo,[b] Masaharu Nishikino,[b] Tetsuya Kawachi,[b] and Yoshinori Shimada[a]

[a]Institute for Laser Technology, Nishi-ku, Osaka, Japan
[b]National Institutes for Quantum and Radiological Science and Technology, Kansai Photon Science Institute, Kizugawa, Kyoto, Japan

Abstract. High-speed laser remote sensing of defects inside a concrete specimen was demonstrated. In the proposed measurement setup, high-power laser pulses irradiated a concrete surface to generate vibration that can be detected by an optical interferometer, which was constructed using photorefractive crystal. The laser-based remote sensing system achieved inspection speeds of 25 Hz. The predominant frequency of a mock-up defect that was embedded in a concrete specimen was measured. The inspection result was identical to that obtained using a conventional hammering method. [DOI: 10.1117/1.JRS.12.015009]

Keywords: laser; remote sensing; concrete; high speed; infrastructure; hammering method.

Paper 170801 received Sep. 10, 2017; accepted for publication Jan. 17, 2018; published online Feb. 9, 2018.

1 Introduction

The degradation of infrastructure (e.g., tunnels) can cause serious accidents. Periodic inspection to detect internal concrete defects using the hammering method is recognized as a major preventive measure to eliminate accidents. However, the hammering method does not provide remote sensing or quantitative evaluation, and it is often time-consuming. It is of key importance to overcome these challenges, in order to improve inspector's safety, reduce human errors, and successfully adapt the inspection methods to various types of infrastructure. Inspection methods for the detection of internal concrete defects employ ultrasound waves,[1–4] thermography,[5–7] and electromagnetic waves,[8–10] which have been proposed to overcome the above challenges. However, taking into account the long track record of the hammering method, further efforts are required to enable large-scale applicability of these methods. Recently, a technique, which employs high-power directional sound source and scanning laser Doppler vibrometer, was proposed.[11,12] A remarkable distinction of this technique, which employs sound source, is the usage of audible detection frequencies, similar to the hammering method. Using the sound source, inspection speed of 0.5 Hz[11] was achieved.

A laser remote sensing (LRS) system, based on the hammering method, has been demonstrated.[13–15] LRS was employed to detect defects in concrete wall of a train-tunnel; the inspection speed was ∼0.5 Hz.[14] Table 1 shows a comparison of the aforementioned methods. The achieved inspection speed was an advantage of the LRS; however, this was not sufficient to outperform the other methods. Prior to improving the disadvantages of the LRS, the advantages should be clearly emphasized. In this study, we developed a high-speed LRS system, which operates at 25 Hz, and demonstrated its ability to detect defects in concrete specimens.

*Address all correspondence to: Shinri Kurahashi, E-mail: kurahashi-shinri@ilt.or.jp

Table 1 Comparison of evaluation methods for defects inside concrete.

Method	Advantage	Disadvantage
LRS (laser hammering)	• Remote sensing	• Effects of the surrounding noise
	• High speed	• Large system
	• Adaptable for curved walls	
Hammering by inspectors	• Lots of records	• Low speed
	• *In-situ* defect treatment	• High-place work
Ultrasonic wave	• Small system	• Low speed
	• High accuracy	• Not suitable for curved walls
		• High-place work
Thermography	• Remote sensing	• Low accuracy
	• Visualization of defects' shapes	• Requires heat source
Electromagnetic waves	• Without traffic restriction	• Almost contact detection

2 Measurement Methods

Figure 1 shows the configuration of the developed LRS system. The LRS system comprises two laser systems: impact laser and detection laser systems. The impact laser system provides high-power laser pulse, which irradiates the concrete surface to generate vibrations, similar as in the human hammering method. The induced vibration is detected by optical interferometer in the laser detection system, which is analogous to human ear. The measurement method is similar to the hammering method. The repetition rates of each of the systems are directly related to the inspection speed.

For a simply supported square concrete plate, its first-order natural frequency f of the induced vibration can be estimated using Eq. (1)[11] as follows:

$$f = \frac{\pi h}{2a^2}\sqrt{\frac{E}{3\rho(1-\nu^2)}}, \tag{1}$$

where h is the thickness of the plate, a is the side length of the plate, E is the Young's modulus, ρ is the density, and υ is the Poisson's ratio. For concrete, $E = 2.27 \times 10^{10}$ Pa, $\rho = 2.30 \times 10^3$ kg/m^3, and $\upsilon = 0.20$. The maximum inspection speed of the LRS system should be smaller than the predominant frequency; if a higher inspection speed is employed, the predominant frequency would not be detected. Therefore, the inspection speed is limited by the targeted defect size (thickness and side length). Figure 2 shows the calculation results of the predominant frequency for a simply supported square concrete plate. Figure 2(a) shows

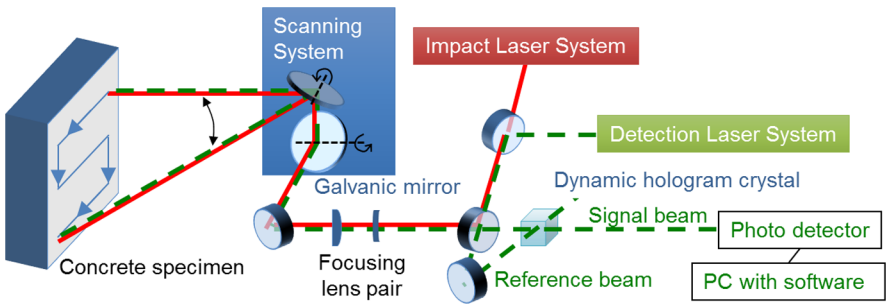

Fig. 1 Configuration of the developed LRS system.

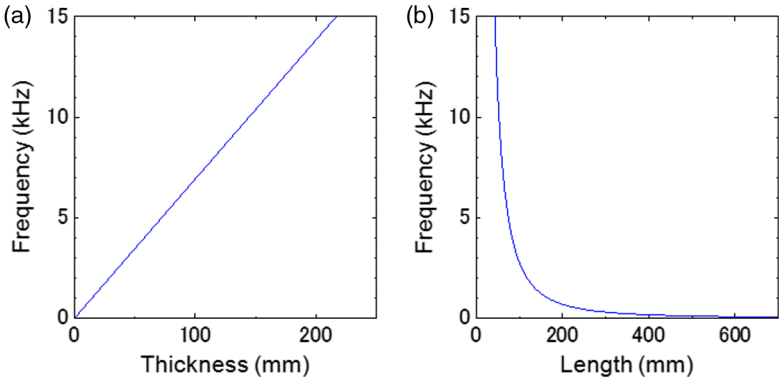

Fig. 2 Calculation results of the predominant frequency of a simply supported square-concrete plate that has constant Poisson's ratio. (a) Thickness dependence ($a = 200$ mm) and (b) side length dependence ($h = 10$ mm), respectively.

the thickness dependence of the frequency, at constant side length of $a = 200$ mm, whereas Fig. 2(b) shows the side length dependence of the frequency, at constant thickness of $h = 10$ mm. The calculation results demonstrate that shallow and wide defects cannot be detected using the employed high inspection speed. The predominant frequency, which can be calculated using Eq. (1), appears as a peak in the vibration spectrum. The reduction of noises, which can appear as another peak, is important in order to emphasize the predominant peak. In the LRS system, the laser-induced vibration on the concrete surface is generated by laser ablation. The laser ablation could generate sound noise, which could decrease the signal-to-noise ratio (SNR), and disturb the vicinity of the laser irradiation area. As the incident laser pulse irradiates the sample, the presence of the sound should be considered, owing to the influence of the acoustic wave on the optical interferometer results; it can decrease the SNR. The acoustic wave comes from the sample, at a distance of 7 m. It reaches the optical interferometer after ~20 ms. Therefore, an inspection speed larger than 50 Hz would be unfavorable for tunnel inspection. The required number of measured points to completely inspect a half-round-shaped tunnel that has a radius of 7 m and length of 1000 m is roughly estimated to be 0.175 million. The estimated inspection time is 2 h, for a grid size of 200 mm and inspection speed of 25 Hz.

3 High-Speed Inspection System

The developed LRS system was configured using three components: impact laser system, detection laser system, and scanning system, as shown in Fig. 1. The LRS system was designed assuming that it will operate in an actual tunnel.

3.1 *Impact Laser System*

Figure 3 shows the optical layout of the impact laser system. The impact laser system was developed using master oscillator power amplifier platform based on the concept of transportable systems.[16] A commercial Q-switched Nd:YAG laser was employed as the master oscillator; its wavelength and pulse width were 1064 nm and 14 ns, respectively. The input power into the amplifier was adjusted using a half-wave plate and polarizer. The laser pulse of the master oscillator was amplified using a Nd:YAG rod amplifier. The concentration of Nd in the rod was 1.1 at%, and the rod size was 14 mm × 70 mm. Two flash lamps formed the pumping source of the Nd:YAG rod; it provides a low running cost and improved stability against environmental variations, such as the external temperature fluctuations. The thermal lens effect, typical issue in the development of high-power laser systems, was observed. It should be corrected, in order to be able to properly focus by the focusing lens pair to achieve strong laser-induced vibration, as shown in Fig. 1. The collection was performed using matching divergence angle by adjusting the distance between the lens pair A, as shown in Fig. 3. Figure 4 shows the performance of

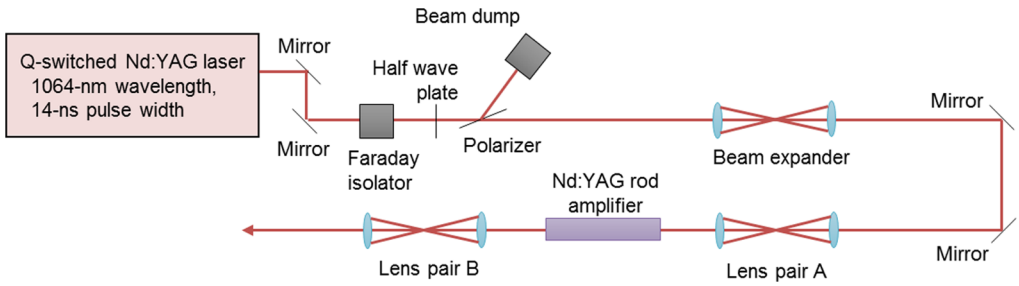

Fig. 3 Optical layout of the developed impact laser system.

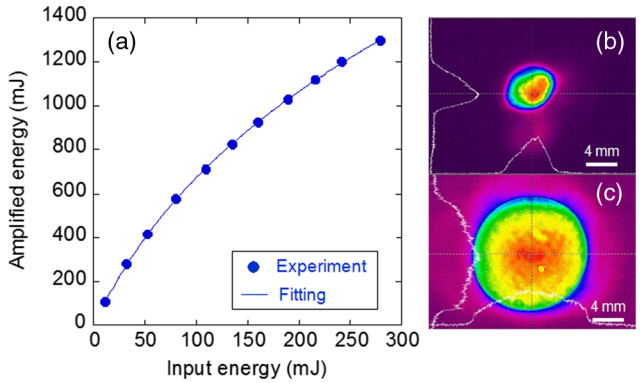

Fig. 4 Performance of the developed impact laser system: (a) input–output characteristics, (b) far-field pattern, and (c) near-field pattern.

the Nd:YAG rod amplifier. The amplified energy reached 1.3 J when the input energy of the master oscillator was ~280 mJ, as shown in Fig. 4(a). The repetition rate was set to 25 Hz. Using the Frantz–Nodvik formula,[17] it was estimated that the small signal gain coefficient and stored energy were 0.328 cm^{-1} and 2.36 J, respectively. The layout of the impact laser system was simple, in order to prevent amplified spontaneous emission (ASE) that would interrupt the laser pulse amplifier. Free-run experiment confirmed that the ASE was small, order of several millijoules. After passing through the Nd:YAG rod amplifier, over 92% of the energy was transferred on the concrete specimen to the far-field pattern, as shown in Fig. 4(b). The developed impact laser system was expected to increase the speed of the LRS system, as demonstrated previously.[14] In addition, the smooth profile appeared in the near-field pattern, as shown in Fig. 4(c), where the beam image was transmitted to the scanning system using the lens pair B, to prevent laser-induced damage of the optical components.

3.2 *Detection Laser System*

The detection laser system was developed using optical interferometer, which was also employed in a previous study.[14] Figure 5 shows the optical layout of the developed detection laser system. The continuous wave laser beam had a wavelength of 532 nm and was split into two beams: a reference beam and a probe beam. The probe beam was focused on the inspected concrete surface and then intersected with the reference beam in the photorefractive crystal, yielding a recordable dynamic hologram.[18] A signal beam that is scattered on a concrete surface contains not only geometric but also laser-induced vibration information. The signal beam generates an interference pattern upon incidence into the photorefractive crystal. In addition, a diffraction grating that corresponds to the brightness and darkness regions of the interference pattern is formed inside the photorefractive crystal; this can be regarded as a hologram. The diffraction grating can be formed by following the changes in the interference fringes; the speed of following depends on the time constant of the photorefractive crystal. This is possible

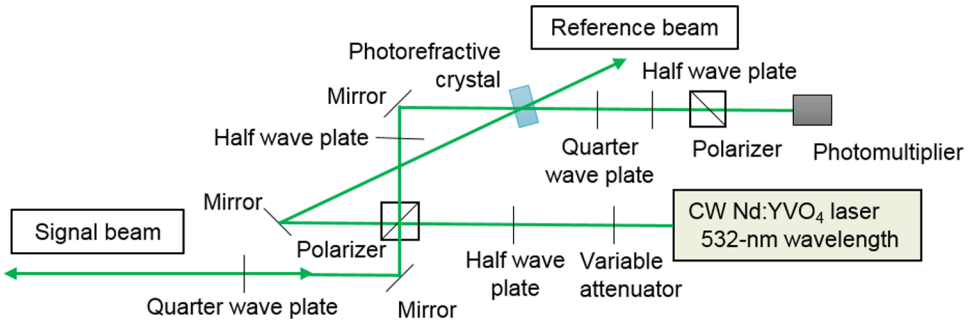

Fig. 5 Optical layout of the developed detection laser system.

owing to the ability to produce a diffraction grating at the photorefractive crystal in advance later moment than the time constant. So, the information of the surface state of the sample was included in the photorefractive crystal. The component that transmits through the grating, of the signal beam which irradiates the photorefractive crystal containing the diffraction grating, and the component of the reference beam that is diffracted by the grating, reach the same wave surface. Therefore, it is possible to extract the information of the excited vibration only from the signal beam. The signal beam was detected using a photomultiplier, while the internal defects inside the concrete specimen were determined using real-time signal analysis. In the analysis, the Fourier-transform spectrum of the homodyne signal was extracted within the audible range. The ratio between the power of the highest peak of the spectrum and average power observed at other frequencies was calculated. In order to check whether a defect exists in the structure, this ratio was compared with the set threshold.

3.3 *Scanning System*

The two laser beams of the impact and detection laser systems were focused on the inspected concrete surface using the lens pairs of each beam scanning system. The distances between the lenses were adjusted to obtain the desired focal length.

The two laser beams were scanned using a pair of galvanic mirrors (QS-30, Nutfield Technology). A SiC substrate that had a desired weight was used for the galvanic mirror, as the associated inertial force had to be reduced to allow precise movement and stoppage.

3.4 *Unified Control System*

High-speed inspection was performed using repetitive cycles through which the beam was first steered to an inspection point using the galvanic mirrors, and then the associated dynamic hologram was recorded at the photorefractive crystal, followed by the acquisition, processing, and analysis of the measured signals. In order to ensure proper and accurate device operation timing, synchronized control was employed using a pulse generator DG645 (Stanford Research Systems) and external master clock. In such a setup, the irradiation timing of the impact laser, movement timing of the galvanic mirrors, and acquisition timing of the detection system have to be controlled.

Figure 6 shows the time chart of the 25-Hz-inspection. The 25-Hz-pulses were generated using the DG645 generator, which had an external master clock. These pulses, along with the start pulses that are provided at any time, were used as inputs to an AND logic gate, which outputs AND signal. Based on this signal, the delay time and pulse duration can be set in each system. For the impact laser, the delay time was 40 ms. With respect to the galvanic mirrors, the delay time was 26 ms and the pulse had a duration of 4 ms. This duration corresponded to the time required to move the galvanic mirrors between consecutive inspection points. For the detection system, the delay time was set to 40 ms, with a pulse duration of 10 ms. This pulse duration corresponded to the time required to acquire the signal. These delayed pulses were supplied at a frequency of 25 Hz and repeated for all inspection points.

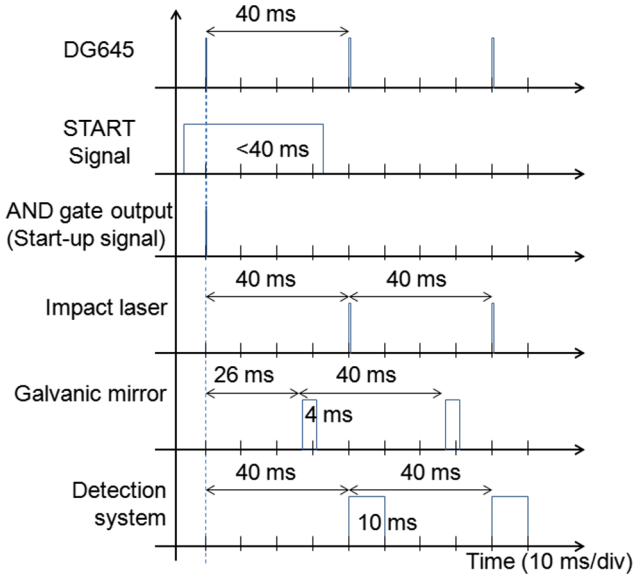

Fig. 6 Time chart of the 25-Hz-inspection method for each device and system.

4 Laser Remote Sensing Measurements and Results

A concrete specimen was set at a distance of 7 m in front of the scanning system's galvanic mirror. Figure 7(a) shows the concrete specimen that had a lateral size of 300×300 mm^2 and thickness of 100 mm. The mock-up defect had a thickness of 5 mm, and it was formed from polystyrene that was embedded at a depth of 10 mm. In the figure, the solid line outlines the defect shape, measured using the hammering method. Figure 7(b) shows the actual LRS system result, superimposed onto the specimen's image. The irradiation energy and spot size of the impact laser beam were 1 J and 5.5 mm (diameter), respectively. The impact and detection laser beams irradiated 7×7 points, separated by 33 mm in both directions. In the figure, each blue dot outlines an inspection point. An image that shows the homodyne signal's analysis results is obtained, where the faint and dark areas indicate the defect-free and defective regions, respectively. Interpolation between the inspected points was used to obtain the result with a color gradation, as shown in Fig. 7(b); the value of each interpolated point was estimated using the output value of the analysis device and relative distances from each of the other inspection points. The color scale in Fig. 7(b) was set by comparison between the ~1.9-kHz peak value and average value in the range of 0.5 to 10 kHz of the frequency spectra, in order to illustrate the known shape of the internal defect. It is worth noting that the setting method of the color scale should be optimized for different situations.

The results of the LRS system measurements showed that the defective area was 25% smaller than the corresponding value obtained using the hammering method. Furthermore, some defect

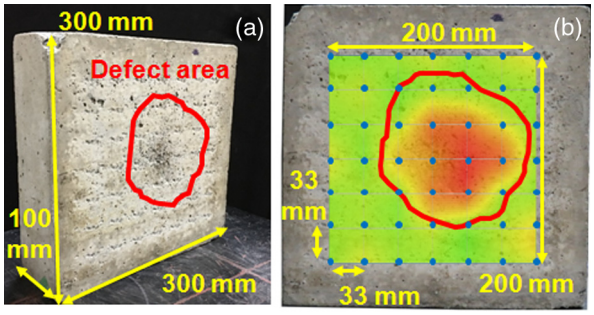

Fig. 7 Demonstration experiment using the LRS system. (a) Image of the concrete specimen. (b) Superimposed inspection result. The red line represents the experimental result measured by the hammering method, while the blue dots represent the inspected points.

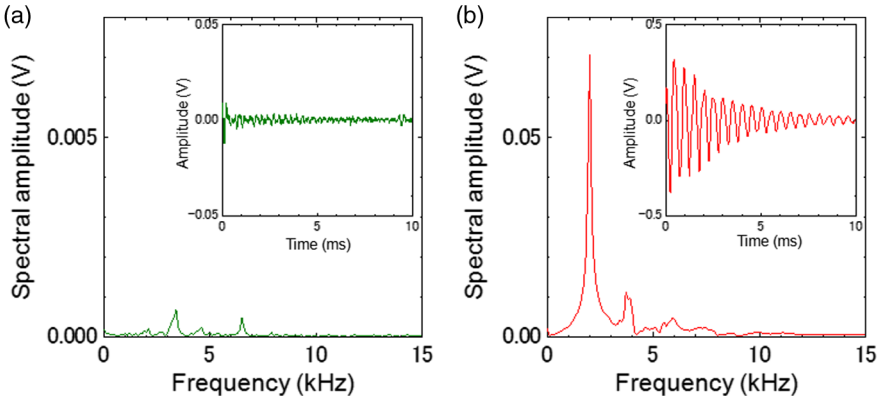

Fig. 8 Frequency spectra and temporal waveforms measured by the hammering and acceleration sensor at areas (a) without defect and (b) with defect, respectively. The values of the longitudinal axes used in the measurements of the defect-free area are one order of magnitude smaller than those of the defective area.

areas evaluated by the human hammering method were not detected by the LRS system, as shown in Fig. 7(b). The defect's edge required more energy to detect the internal defects than that required for the central part. Therefore, the enhancement of the impact laser beam is important. In the hammering method, the impact interval was ~20 mm, which became narrower at the vicinity of the edge. Accordingly, reducing the distance between inspected points is advantageous for obtaining a higher accuracy for the prediction of defective edges.

The inspection results obtained by the LRS system were compared to those obtained using the hammering technique. Figure 8 shows the frequency spectra and temporal waveforms measured using the human hammering method and acceleration sensor (NP-3211, Ono Sokki Co., Ltd.) at (a) defect-free [uppermost left point in Fig. 6(c)] and (b) defective [central blue dot in Fig. 6(c)] regions. The signal amplitude of the defect-free region was smaller than that of the defective region, as shown in Fig. 8(b), which seemed to be lower than the noise level. The typical peak appeared around 1.9 kHz, as shown in the frequency spectrum of the defective area [Fig. 8(b)]. According to Eq. (1), this frequency value justifies the assumption that the first-order natural frequency of the induced vibration within the defective area can be detected. A peak around 3.6 kHz also appeared and it seems that corresponds to a vibration of (1, 2)-order and/or (2, 1)-order mode. On the other hand, Fig. 9 shows the frequency spectra and homodyne signal measured by the LRS system, at the same points presented in Fig. 8. The results of the LRS system measurements were identical to those measured using the hammering method. The ratio between the ~3.6 and 1.9 kHz peaks was different compared with that obtained using the human hammering method. The difference might be caused by the fluctuations of the hammering points. Therefore, for the LRS, a single peak should be used to determine the presence of a defect

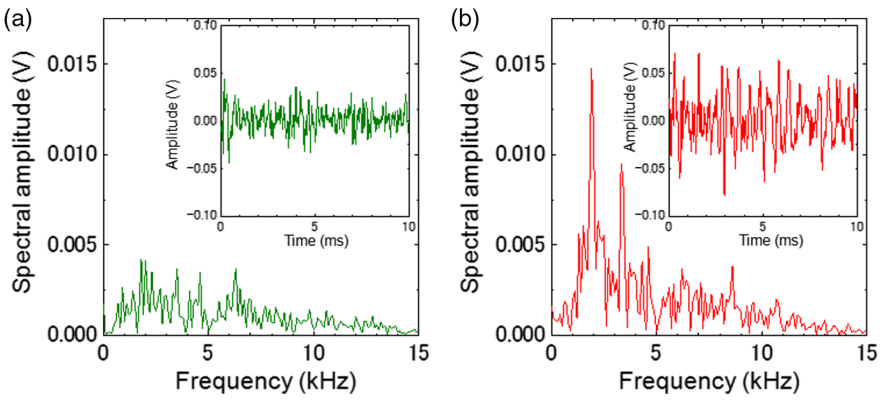

Fig. 9 Frequency spectra and temporal waveforms measured using the LRS system at the (a) defect-free and (b) defective areas, respectively.

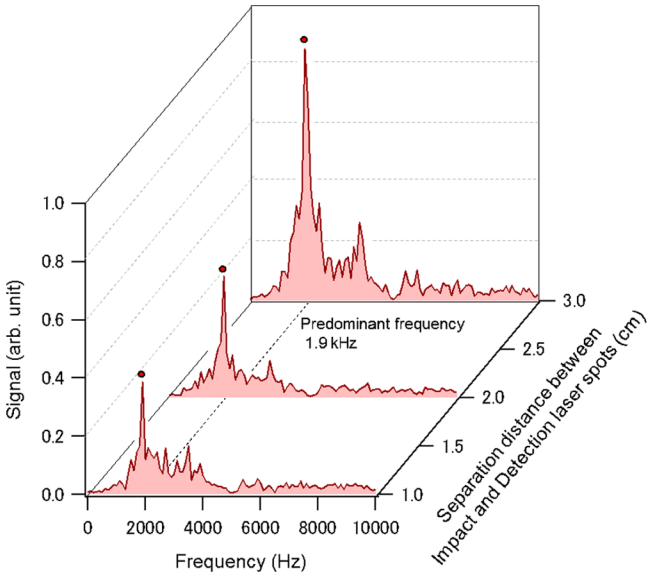

Fig. 10 Frequency spectra for different distances between the impact and detection laser spots.

inside another defect. In addition, the spectral amplitude of the defective regions was larger than that of the defect-free regions, with a typical peak appearing around 1.9 kHz. This implies that the present laser technology can drastically improve the human-based hammering method.

The LRS results are influenced by the conditions of the impact and detection lasers. Figure 10 shows the frequency spectra for different distances between the impact and detection laser spots, when the same point was measured, as shown in Fig. 9(b). The vibration was caused by the surface ablation of the concrete. The dust, plasma emission, and shot sound when the ablation occurred, contributed to the measurement noise. Therefore, the signals intensities increased with the distance between the impact and detection laser spots. On the other hand, the separation of

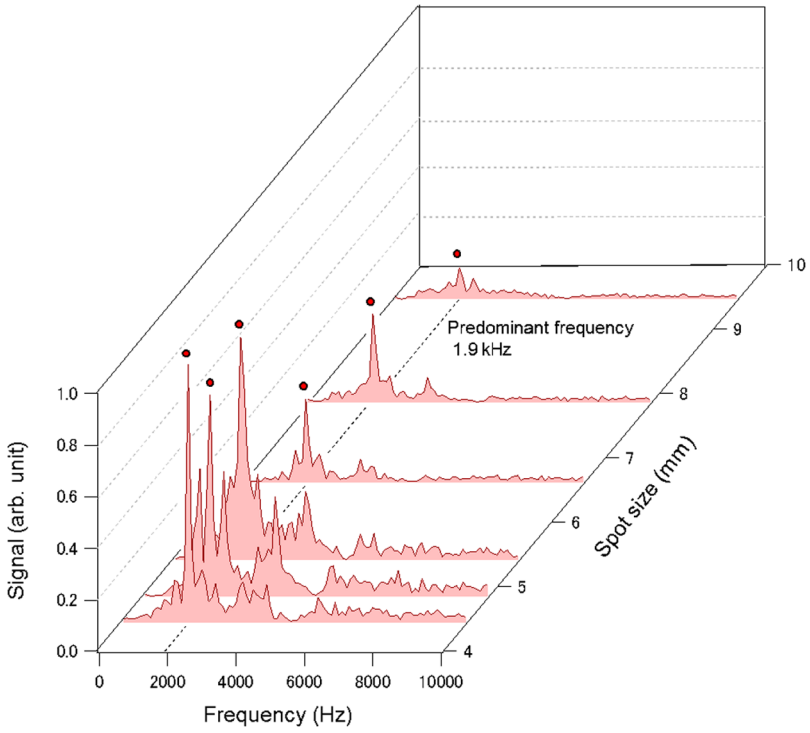

Fig. 11 Frequency spectra for different spot sizes of the impact laser.

these spots caused mismatch between the impact and detection points. Therefore, the spatial resolution is limited by the separation distance. Trade-off solution should be proposed based on the spatial resolution; the separation distance in the measurements was 3 cm, as shown in Fig. 9(b). The spot size of the impact laser beam determines the irradiation fluence, and the signal intensity affects the laser-induced vibration process through the ablation phenomenon. Figure 11 shows the frequency spectra for different spot sizes of the impact laser beam, which had a pulse energy of 1 J, recorded at the same measurement point as that in Fig. 9(b). Smaller spot size, i.e., high-fluence, could provide larger signals than those obtained using larger spot size. Therefore, a high-fluence irradiation of the impact laser is effective for the LRS system.

5 Conclusion

We developed high-speed inspection laser system for the detection of internal defects in concrete. Using a mock-up concrete specimen, it was demonstrated that the LRS technique at an inspection speed of 25 Hz yielded identical results to those obtained using the hammering method. This result signifies dramatic improvement in inspection speed using the proposed laser technology. In future studies, the proposed high-speed inspection system should be improved in order to achieve an inspection speed of 50 Hz. In particular, it should be aimed to implement multipass amplifiers in the impact laser system to increase the output energy for the excitation of larger vibration response. In addition, the detection laser system should be achieved higher speed and enhanced sound noise insulation, which will increase the SNR.

Acknowledgments

This study was supported by the "Development of high-specification nondestructive inspection method for infrastructure constructions with laser technology" project (representative: Dr. Katsumi Midorikawa, RIKEN) at the Council for Science, Technology, and Innovation, "Cross-ministerial Strategic Innovation Promotion Program (SIP), Infrastructure Maintenance, Renovation, and Management," funded by Japan Science and Technology Agency (JST). We would like to thank Dr. Norikazu Misaki (West Japan Railway Company) and Dr. Masahiro Shinoda (National Defense Academy of Japan) for their insightful comments and suggestions.

References

1. V. N. Kozlov, A. A. Samokrutov, and V. G. Shevaldykin, "Thickness measurements and flaw detection in concrete using ultrasonic echo method," *Nondestr. Test. Eval.* **13**(2), 73–84 (1997).
2. M. Schiclert, M. Krause, and W. Müller, "Ultrasonic imaging of concrete elements using reconstruction by synthetic aperture focusing technique," *J. Mater. Civ. Eng.* **15**(3), 235–246 (2003).
3. K. Hoegh et al., "Ultrasonic linear array validation via concrete test blocks," in *AIP Conf. Proc.*, Vol. 1650, pp. 83–93 (2015).
4. H. Choi and J. S. Popovics, "NDE application of ultrasonic tomography to a full-scale concrete structure," *IEEE Trans. Ultrason. Ferroelectr. Freq. Control* **62**(6), 1076–1085 (2015).
5. M. R. Clark, D. M. McCann, and M. C. Forde, "Application of infrared thermography to the non-destructive testing of concrete and masonry bridges," *NDT&E Int.* **36**(4), 265–275 (2003).
6. C. Maierhofer et al., "Application of impulse-thermography for non-destructive assessment of concrete structures," *Cem. Concr. Compos.* **28**(4), 393–401 (2006).
7. C. Meola, "A new approach for estimation of defects detection with infrared thermography," *Mater. Lett.* **61**(3), 747–750 (2007).
8. O. Büyüköztürk and H. C. Rhim, "Rader imaging of concrete specimens for non-destructive testing," *Constr. Build. Mater.* **11**(3), 195–198 (1997).

9. K. J. Langenberg, K. Mayer, and R. Marklein, "Nondestructive testing of concrete with electromagnetic and elastic waves: modeling and imaging," *Cem. Concr. Compos.* **28**(4), 370–383 (2006).
10. P. Owerko, Ł. Ortyl, and M. Salamak, "Identification of concrete voids in an untypical railway bridge pillar by ground penetrating radar method," *Meas. Autom. Monit.* **61**(3), 76–80 (2015).
11. R. Akamatsu et al., "Proposal on non-contact inspection method for concrete structure using high-power directional sound source and scanning laser Doppler vibrometer," *Jpn. J. Appl. Phys.* **52**(7S), 07HC12 (2013).
12. K. Sugimoto et al., "Defect-detection algorithm for noncontact acoustic inspection using spectrum entropy," *Jpn. J. Appl. Phys.* **54**(7S1), 07HC15 (2015).
13. O. Kotyaev and S. Uchida "Nondestructive inspection of concrete structures with the use of photorefractive two-wave mixing," *Proc. SPIE* **4702**, 241–249 (2002).
14. O. Kotyaev, Y. Shimada, and K. Hashimoto, "Laser-based non-destructive detection of inner flaws in concrete with the use of lamb waves," in *European Conf. for Non Destructive Testing*, pp. 25–29 (2006).
15. Y. Shimada and O. Kotyaev, "Remote sensing of concrete structure using laser sonic waves," in *Industrial Application of Laser Remote Sensing*, T. Fukuchi and T. Shiina, Eds., pp. 153–169, Bentham Science, Sharjah (2012).
16. K. Mikami et al., "Flash-lamp-pumped 4 J, 50 Hz Nd:YAG nanosecond laser system for mobile and transportable equipment," *Jpn. J. Appl. Phys.* **56**(8), 082701 (2017).
17. L. M. Frantz and J. S. Nodvik, "Theory of pulse propagation in a laser amplifier," *J. Appl. Phys.* **34**(8), 2346–2349 (1963).
18. R. K. Ing and J. P. Monchalin, "Broadband optical detection of ultrasound by two-wave mixing in a photorefractive crystal," *Appl. Phys. Lett.* **59**(25), 3233–3235 (1991).

Shinri Kurahashi received his PhD in engineering from Osaka University in 2017. He has been involved for 7 years in developing a remote inspection system for concrete structures using lasers.

Biographies for the other authors are not available.